

# A Dual-Source Attention Transformer for Multi-Person Pose Tracking

Andreas Doering and Juergen Gall

University of Bonn

**Abstract.** Multi-person pose tracking is an important element for many applications and requires to estimate the human poses of all persons in a video and to track them over time. The association of poses across frames remains an open research problem, in particular for online tracking methods, due to motion blur, crowded scenes and occlusions. To tackle the association challenge, we propose a Dual-Source Attention Transformer that incorporates three core aspects: i) In order to re-identify persons that have been occluded, we propose a pose-conditioned re-identification network that provides an initial embedding and allows to match persons even if the number of visible joints differs between the frames. ii) We incorporate edge embeddings based on temporal pose similarity and the impact of appearance and pose similarity is automatically adapted. iii) We propose an attention based matching layer for pose-to-track association and duplicate removal. We evaluate our approach on Market1501, PoseTrack 2018 and PoseTrack21.

## 1 Introduction

Multi-person pose tracking is highly relevant for a wide range of applications such as virtual reality, autonomous driving or sports analysis and requires to accurately estimate and track the human poses of all persons throughout a video. Despite of the recent progress in multi-person pose tracking [37, 12, 22, 13, 42, 54, 38, 55, 49], the task remains very challenging due to camera motion, motion blur, occlusions, and a high variety in pose and scale [11]. Consequently, a tracking approach must be robust to detection errors and ambiguities. In particular, the assignment of highly occluded persons in unusual poses is very difficult as shown in Fig. 1 where three persons perform a gymnastic exercise in water. For instance, the green bounding box intersects with three persons and the respective pose overlaps with the keypoints of the other persons. This poses a challenge, especially for on-line methods as assignments will be made once a new frame arrives.

Related works such as [42, 38, 55, 54, 63] try to tackle these challenges by generating future poses from a track’s history, which are then matched with detections based on pose similarities, *e.g.*, based on Object Keypoint Similarity (OKS) [38, 54, 63] or a pose-based matching layer [42]. Other works such as [49] process each sequence in an off-line fashion, which is not feasible for real-time applications. As these works mainly rely on pose-based similarities for matching,

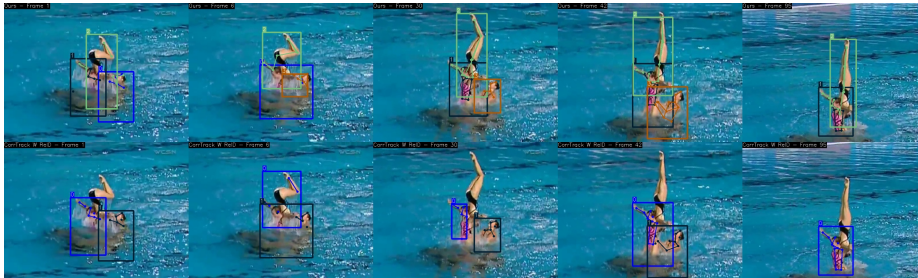


**Fig. 1.** Qualitative examples of our proposed method on the PoseTrack21 dataset. The first row contains visual tracking results of our method and the second row shows visualizations of CorrTrack with ReID [11].

these methods tend to fail to re-identify tracks that have been occluded for longer periods of time or undergo high pose deformations.

In our work, we thus focus on learning the association of detected persons to tracks in an on-line fashion and propose an approach that leverages the estimated poses, bounding boxes, and the appearance of the detected persons to assign them to previous tracks or initialize new tracks. Since we can neither rely solely on appearance-based features nor pose similarities due to multiple instances with similar appearance, changing camera views or scene switches, which often occur in in-the-wild sequences, we propose a dual-source transformer that considers the similarity between detection embeddings and previous track embeddings as well as edge embeddings that encode temporal pose similarities. All three embeddings are updated by a dual-source decoder and a final matching layer assigns the detections to the tracks. The matching layer also removes duplicates, *i.e.*, multiple detections for the same persons, and initiates new tracks. Furthermore, we propose a pose-conditioned re-identification model where the appearance features are normalized based on the heatmaps of the detected keypoints. Our model is more robust to occlusions in crowded scenarios compared to related works such as [45, 33] that solely operate on a bounding-box level.

We evaluate our approach on the challenging PoseTrack 2018 [1] and PoseTrack21 dataset [11] where it achieves state-of-the-art results. Moreover, we evaluate our pose-conditioned appearance model for the task of person re-identification on the Market1501 dataset [62], where we achieve competitive results with the current state-of-the-art. In summary, we propose (1) a novel pose-conditioned re-identification model for human pose tracking, (2) a dual-source attention transformer that combines pose and appearance similarity in a novel way for pose-to-track association and (3) a novel matching layer for pose-to-track association and duplicate removal.

## 2 Related Work

We briefly discuss some related works for person re-identification and multi-person pose tracking.

*Person Re-Identification:* Methods for person re-identification aim to generate robust feature representations of a query person, which allows to re-identify each instance of the particular person. These methods can be divided into different categories such as re-identification based on global features [33, 20], part-based approaches [45, 25, 44], prior-based, *i.e.*, pose- or mask-guided [14, 40, 61, 53, 36] and video-based [5, 6, 26] re-identification. Part-based models [45, 25, 44] divide each image into several parts and extract distinct part-based features. Features for each part are either trained individually [45] or further re-combined to obtain visibility-aware features [44]. Pose- [14, 40, 61, 53] or mask-guided [36] approaches aim to suppress background-noise by learning occlusion- and instance-aware features that are more robust in crowded scenarios with occlusions. In this work, we propose Spatially Adaptive Pose DEnormalization (SPAPDE) layers for pose-guided re-identification and use it in the proposed dual-source tracking transformer.

*Multi-Person Pose Tracking:* Existing works on multi-person pose tracking can be divided into two categories: top-down methods [55, 49, 42, 38, 11, 63, 57] and bottom-up methods [37, 22, 13, 12]. Former approaches employ a person detector and estimate the pose for every detected person individually based on temporal-context. Most methods employ a pose-warping [38, 11, 57] scheme that warps tracked poses into the next frame or directly predict poses based on the tracklet history [55, 42, 63, 24, 12], which are then matched with detected poses using greedy or Hungarian matching. In [49], an offline approach has been proposed that merges multiple overlapping fixed-lengths tracklets into tracks based on bipartite matching and Dijkstra’s algorithm [10]. Bottom-up approaches [37, 22, 24, 12], on the other hand, predict all keypoints within an image simultaneously and generate tracks by solving spatio-temporal graphs between detected keypoints. For instance, [37, 12, 22] generate spatio-temporal vector fields, while various spatio-temporal embeddings for the association of keypoints and tracks are proposed in [24]. In contrast, person instances are tracked in [13] using a semi-supervised approach based on video instance correspondences. In this work, we propose a Dual-Source Transformer that considers the similarity between detection embeddings and previous track embeddings as well as edge embeddings that encode spatial and pose similarities.

## 3 Dual-Source Attention Transformer for Multi-Person Pose Tracking

On-line methods for multi-person pose tracking often follow the tracking-by-detection paradigm [42, 15, 12, 37, 22, 54, 59, 38] and usually suffer from ambiguities and occlusions. An example is shown in the second row of Fig. 1 where the blue id jumps between two persons. In this work, we thus focus on learning

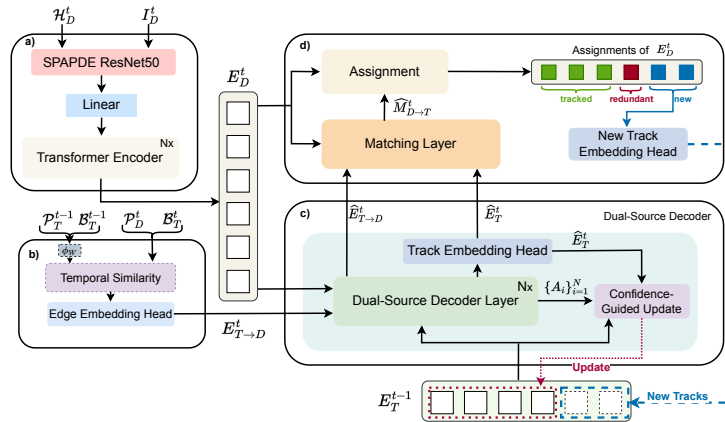


**Fig. 2.** The proposed multi-person pose tracking architecture entails the following steps: a) Given a set of person crops and their respective keypoint heatmaps at time frame  $t$ , we compute pose-conditioned appearance features and feed them into  $N$  transformer encoder stages. This gives an embedding for each detection  $E_D^t$ . b) We also compute temporal similarities between tracks and detected persons by means of Intersection over Union (IoU) and Object Keypoint Similarity (OKS), which we then encode into an edge embedding  $E_{T \rightarrow D}^t$ . c) The dual-source decoder takes the embeddings of the previous tracks  $E_T^{t-1}$ , the detection embeddings  $E_D^t$  and the edge embeddings  $E_{T \rightarrow D}^t$  as input and updates the embeddings. d) Finally, the matching stage assigns detections to tracks, removes redundant detections and initializes new tracks.

robust assignments between estimated poses in a current frame and tracked persons in previous frames. This is done by the proposed dual-source transformer that combines appearance features and encoded temporal person similarities. Since the importance of appearance and pose similarity varies within a video and between videos, in particular when a person has been occluded for a few frames, the dual-source decoder and the matching layer use a gating mechanism to update the embeddings of the new poses and previous tracks and to match poses to tracks. Our approach for multi-person pose tracking is illustrated in Fig. 2.

We assume that the human poses are extracted for a new frame  $t$  by a standard multi-person pose estimator where we utilize the detector from [11] for a fair comparison. Specifically, for a given frame at time  $t$ , our network takes as input the set of estimated bounding boxes  $\mathcal{B}_D^t$  and poses  $\mathcal{P}_D^t$ , and additionally detected keypoint heatmaps  $\mathcal{H}_D^t$  extracted from the image crops  $\mathcal{I}_D^t$  of detected persons. From the heatmaps and image crops, an embedding  $E_D^t$  for re-identification will be computed as described in Section 3.2 (Fig. 2a). To measure pose and spatial proximity between detections and tracks, similarities to the bounding boxes  $\mathcal{B}_T^{t-1}$  and poses  $\mathcal{P}_T^{t-1}$  of the last frame of each track are predicted, which results in the embedding  $E_{T \rightarrow D}^t$  (Fig. 2b) that will be described

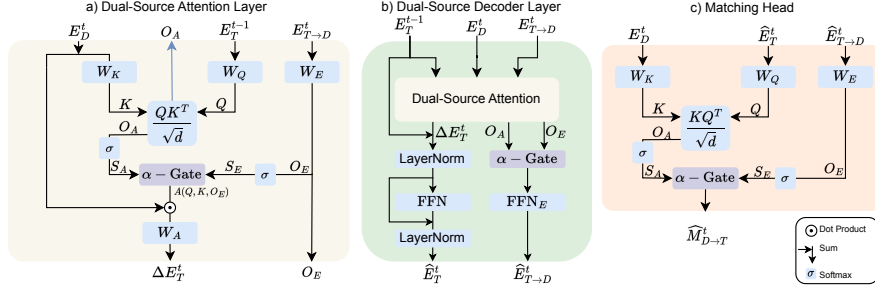


**Fig. 3.** Illustration of our proposed a) Dual-Source Attention layer, b) Dual-Source Decoder layer and c) the Matching layer. The Dual-Source Decoder layer takes as input the detection embeddings  $E_D^t$ , track embeddings  $E_T^{t-1}$  and edge embeddings  $E_{T \rightarrow D}^t$  and updates the track embeddings  $\hat{E}_T^t$  and edge embeddings  $\hat{E}_{T \rightarrow D}^t$  using the Dual-Source Attention layer. The matching layer predicts an assignment matrix  $\hat{M}_{D \rightarrow T}^t$  of detections to tracks. The  $\alpha$ -Gates fuse the cross-attention matrix  $S_A$  between detections and tracks, which measures appearance similarity, and the self-attention matrix  $S_E$  of the edge embeddings, which measures spatial and pose similarity.

in Section 3.2 as well. Similar to [16], we call  $E_{T \rightarrow D}^t$  edge embedding since it is an embedding of the edges between the tracks and detections. Given both embeddings  $E_D^t$  and  $E_{T \rightarrow D}^t$  as well as the track embeddings  $E_T^{t-1}$  that have been estimated in the previous frame  $t-1$ , the proposed *Dual-Source Decoder* (Fig. 2c) and the *Matching Layer* (Fig. 2d) assign the current detections to previous tracks, update the track embeddings, and initialize new tracks. Both will be described in the following Section 3.1.

### 3.1 Dual-Source Decoder

*Dual-Source Attention Layer* The main components of our proposed dual-source transformer are the dual-source attention layers and the matching layer. As illustrated in Fig. 3a, the dual-source attention layer combines appearance-based similarities  $S_A = \sigma(O_A)$  and embedded temporal pose similarities  $S_E = \sigma(O_E)$  between detections and tracks, where  $\sigma$  is the row-wise softmax layer. While the pose similarity logits  $O_E = E_{T \rightarrow D}^t W_E^T$  are obtained by  $E_{T \rightarrow D}^t$  and the learned weight matrix  $W_E$ , the appearance-based similarity logits  $O_A$  are obtained by cross-attention between the appearance features of the detections  $E_D^t$  and tracks  $E_T^{t-1}$ :

$$O_A = \frac{E_T^{t-1} W_Q^T (E_D^t W_K^T)^T}{\sqrt{d}}. \quad (1)$$

where  $W_Q$  and  $W_K$  are the learned projection weights for the queries and keys, respectively, and  $d$  is the dimensionality of the embeddings  $E$ .

In order to assign detections to tracks, appearance-based similarities  $S_A$  and embedded temporal pose similarities  $S_E$  are fused by the  $\alpha$ -Gate that weights

the contribution of appearance-based attention weights and the pose-based attention weights by a hyperparameter  $\alpha$ , which we evaluate in our experiments:

$$A = \alpha \cdot S_A + (1 - \alpha) \cdot S_E. \quad (2)$$

Intuitively, pose and spatial similarities  $S_E$  provide a strong matching prior, but are less reliable in crowded scenarios as shown in Fig. 1. Appearance similarities  $S_A$  allow to re-identify an occluded person after some frames, but are unreliable in case of motion blur or person instances with similar appearance as it is common in team sport videos. While none of them can resolve all ambiguities, fusing the normalized similarities  $S_A$  and  $S_E$  automatically gives higher weight to the similarity measure where the matching confidence of a detection to a track is higher. This, however, only works if also we allow that none of the detections is assigned to a track, *e.g.*, if a person has not been detected or is occluded. Prior to applying the softmax to the attention matrices, we thus add a column of zeros. In other words, the last column of  $S_A$  and  $S_E$  indicates if a track does not match with any detection.

Finally, the dual-source attention layer calculates a proposed track embedding update as follows:

$$\Delta E_T^t = (A_{:, :-1} E_D^t) W_A^\top, \quad (3)$$

where  $A_{:, :-1}$  denotes the attention weights without the last column and  $W_A$  are the weights of a linear layer.

*Dual-Source Decoder Layer* The dual-source decoder layer shown in Fig. 3b then updates the track  $E_T^{t-1}$  and edge  $E_{T \rightarrow D}^t$  embeddings based on the output of the dual-source attention layer. As common for transformer blocks [47], we use a residual feed-forward network (FNN) as shown in Fig. 3b). Specifically, we compute

$$\widehat{E}_T^t = \text{LN}(\widetilde{E}_T^t + \text{FFN}(\widetilde{E}_T^t)), \quad \widetilde{E}_T^t = \text{LN}(E_T^{t-1} + \Delta E_T^t), \quad (4)$$

where LN denotes layer normalization. As shown in Fig. 2c, we employ an additional *Track Embedding Head* after the last decoder layer that predicts the final track embeddings. The *Track Embedding Head* consists of two linear layers, where the first layer comprises LayerNorm [2] and GELU [19] non-linearities.

To update the edge embeddings, we employ an  $\alpha$ -*Gate* to weight the contribution of appearance-based and edge-based attention logits  $O_A$  and  $O_E$  similar to the dual-source attention layer. We then apply a feed-forward network  $\text{FFN}_E$  on the weighted sum of attention logits,

$$\widehat{E}_{T \rightarrow D}^t = \text{FFN}_E(\alpha \cdot O_A + (1 - \alpha) \cdot O_E), \quad (5)$$

where  $\text{FFN}_E$  is a feed-forward network as  $\text{FFN}$ .

*Confidence-Guided Track Update* As shown in Fig. 2c, we perform the final update of the tracks embedding before the final assignment of detections to tracks is done by the matching layer (Fig. 2d). This is done for two reasons. Firstly,

the final assignment might be wrong and, secondly, we do not want to update the track embedding when the detection embedding is noisy due to occlusion or motion blur. To prevent track embeddings from being updated by noisy or low-confident detections, we employ a confidence-guided update of the track embeddings. Let  $\mathcal{A} = \{A_{:,i}^n\}_{n=1}^N$  be the set of dual-source attention weights of all  $N$  decoder stages, without the last column. As the number of detections per frame is dynamic, we apply max pooling on the rows of each attention matrix to obtain the maximum attention score for each track and estimate an importance weight  $w_j$  with a linear layer as

$$\widehat{\mathcal{A}}_j = \text{concat}\{\max_i A_{ji}^n | n \in [1, N]\} \quad (6)$$

$$w_j = \sigma\left(\sum_n w_n \cdot \widehat{\mathcal{A}}_j^n + b_n\right), \quad (7)$$

where  $\sigma$  is the sigmoid function and  $\widehat{\mathcal{A}}_j^n$  the maximum attention for track  $j$  at layer  $n$ . Ultimately, we update the embedding for each track  $j$  as a confidence-guided moving average by using the importance weight  $w_j$  following  $E_{T_j}^t = (1 - w_j) \cdot E_{T_j}^{t-1} + w_j \cdot \widehat{E}_{T_j}^t$ . As we will show in our experiments, the confidence-guided embedding update improves the performance compared to solely relying on the *Track Embedding Head* (Fig. 2c) while only adding a negligible overhead.

*Matching Layer* The matching layer (Fig. 3c) comprises a structure similar to the dual-source attention layer, but differs in two aspects. 1) Unlike the dual-source attention layer, the matching layer does not use the attention weights to predict a track embedding update and therefore does not consist of a linear layer after the  $\alpha$ -Gate. 2) The attention weights (2) are used as assignment matrix  $\widehat{M}_{D \rightarrow T}^t$  to assign detections to tracks, as we show in Fig. 2d). In the presence of duplicate detections, this allows to match multiple detections to a single track. Given the matching matrix  $\widehat{M}_{D \rightarrow T}^t$ , we utilize Hungarian matching to assign detections and tracks. All the remaining detections  $i$  that have a matching probability  $\hat{m}_{i \rightarrow j} > \tau_{dup}$  for any track  $j$  are considered as duplicate detections and are removed. Any other detection will be passed to the *new track embedding head* and initialize a new track embedding (Fig. 2d). The new track embedding head has the same structure as the *track embedding head*. All tracks that have not been tracked for  $\tau_{age}$  frames will be removed. We evaluate the impact of  $\tau_{dup}$  and  $\tau_{age}$  in the experiments.

### 3.2 Encoder Stage

*Pose-Conditioned Appearance Features* Multi-person pose tracking in crowded real-world scenarios is particularly challenging due to many occlusions, especially for appearance-based associations as two persons in close proximity are likely to share similar features. Towards this end, we employ a ResNet50 [17] as our backbone network (Fig. 2a) that we pre-trained for person re-identification

[33]. Since we need to deal with diverse poses and occlusions, we propose a modification to the ResNet and condition the backbone on the keypoint heatmaps  $\mathcal{H}_D^t$  of the pose estimator. Specifically, we propose a Spatially Adaptive Pose DE-normalization (SPAPDE) layer, which is inspired by [35]. Each SPAPDE layer operates on a set of keypoint heatmaps  $\mathcal{H}_D^t \in \mathbb{R}^{N \times K \times \frac{256}{s} \times \frac{128}{s}}$  along with the current ResNet features  $f \in \mathbb{R}^{N \times C \times \frac{256}{s} \times \frac{128}{s}}$  extracted from the corresponding image crops  $\mathcal{I}_D^t \in \mathbb{R}^{N \times 3 \times 256 \times 128}$ , where  $N$  is the number of persons in frame  $t$ ,  $s$  denotes the respective scaling factor,  $K$  denotes the number of keypoints and  $C$  denotes the number of feature channels.

In contrast to batch normalization [23], the normalized input features are scaled and shifted with respect to the keypoint heatmaps. In particular, SPAPDE computes the modulation parameters  $\beta$  and  $\gamma$  following

$$\gamma = \text{conv}(a), \quad \beta = \text{conv}(a), \quad a = \text{ReLU}(\text{conv}(\mathcal{H}_D^t)), \quad (8)$$

where  $\text{conv}$  denotes a 3x3-convolution and  $\beta, \gamma \in \mathbb{R}^{N \times C \times \frac{256}{s} \times \frac{128}{s}}$ . The image features  $f$  are then conditioned on the heatmaps  $\mathcal{H}_D^t$  as follows. Let  $f_{n,c,y,x}$  be the feature value for the detected person  $n$  and feature channel  $c$  at pixel location  $(x, y)$ . The SPAPDE layer first calculates the mean  $\mu_c$  and standard deviation  $\sigma_c$  over all persons and pixels of  $f$  and then adaptively de-normalizes the image features by

$$\hat{f}_{n,c,y,x} = \gamma_{n,c,y,x} \cdot \frac{f_{n,c,y,x} - \mu_c}{\sigma_c} + \beta_{n,c,y,x}. \quad (9)$$

We replace every batch normalization layer within ResNet50 by SPAPDE layers and train the network following [33].

Moreover, we use a vanilla N-stage transformer encoder [47] without positional encoding to further disentangle the backbone features of severely occluded persons and noisy pose predictions and generate a set of encoded person features  $E_D^T \in \mathbb{R}^{N \times 256}$  as shown in Fig. 2a.

*Temporal Edge Features* The edge features  $E_{T \rightarrow D}^t$  (Fig. 2b) used in our dual-source architecture are based on similarities between bounding boxes and poses using Intersection over Union (IoU) and Object Keypoint Similarity (OKS), respectively. In this work, we rely on three variants of OKS: the first variant considers keypoints which are present in both poses. While the first variant provides a good measure of keypoint alignment, its expressiveness suffers if two poses only share a small subset of keypoints. For that reason, the remaining two variants consider all keypoints present in one of the two poses, respectively. OKS denotes thus a 3d vector.

We leverage a warping function  $\phi_W$  to warp all tracks into the current frame  $t$  and calculate the temporal edge features  $E_{T \rightarrow D}$  between tracks and detections as follows:

$$E_{T \rightarrow D} = \phi_E \left( \left[ IOU(\hat{\mathcal{B}}_T^{t-1}, \mathcal{B}_D^t) \parallel OKS(\hat{\mathcal{P}}_T^{t-1}, \mathcal{P}_D^t) \right] \right). \quad (10)$$

Here,  $\hat{\mathcal{P}}_T^{t-1} = \phi_W(\mathcal{P}_T^{t-1})$  and  $\hat{\mathcal{B}}_T^{t-1} = \phi_W(\mathcal{B}_T^{t-1})$  represent the set of warped track poses and track bounding boxes, respectively. The operator  $[\cdot \parallel \cdot]$  represents



concatenation, and  $\phi_E$  denotes the edge embedding head, which consists of three linear layers with LayerNorm [2] and GELU [19].

### 3.3 Training Objective

In a first step, we train the re-identification network following [33]: We apply the triplet loss [20] and center loss [53] after the last pooling layer of ResNet50 and we employ the cross-entropy loss with label smoothing [46] on the classification layer. Subsequently, we freeze the re-identification network and proceed to train our dual-source transformer.

In our approach, the matching layer is trained using a cross-entropy loss, which is defined as follows:

$$\mathcal{L}_{match} = -\frac{1}{N_D} \sum_i y_i \cdot \log(p_{ij}^m) + (1 - y_i) \cdot p_{i0}^m, \quad (11)$$

where  $N_D$  is the total number of detections,  $p_{i,j}^m$  represents the probability of matching the  $i$ -th detection to its corresponding ground truth track  $j$ , and  $p_{i0}^m$  is the probability of not matching the  $i$ -th detection to any track. The variable  $y_i$  takes the value 1 if the  $i$ -th detection is assigned to a ground truth track and 0 otherwise.

To optimize the performance of our approach, we provide direct feedback to both the encoder and decoder, thereby enabling maximum guidance during the training process. Since we discard duplicates after the final matching layer, we intentionally integrate duplications into the training process and allow multiple detection assignments to a single track. Specifically, we leverage both, detected poses and ground truth poses in the training process that can share the same person identity. To assign identities to the detected poses we employ OKS-based greedy matching to the ground truth poses. We then utilize a duplicates-aware cross-entropy loss function that operates on the attention weights of the encoder and decoder layers. The loss function is defined as follows:

$$\mathcal{L}_{attn} = -\frac{1}{N_T} \sum_j \log(p_j), \quad p_j = \left( \sum_i A_{ji} \mathbb{I}_i(j) \right) + \mathbb{I}_{\#i}(j) A_{j0}. \quad (12)$$

$N_T$  represents the total number of tracks and  $p_j$  denotes the accumulated matching probability for track  $j$ , where  $A_{ji}$  is the attention weight of the respective encoder/decoder layer and  $\mathbb{I}_i(j)$  is 1 if the identity of the current track  $j$  and the detection  $i$  are the same, and 0 otherwise. If none of the detections matches, *i.e.*,  $\mathbb{I}_{\#i}(j)$ , we maximize the no-match probability  $A_{j0}$ , which is the last column of the attention matrix as discussed in Section 3.1. In other words, we want that  $A_{ji}$  is large for the correct assignment if and only if a match exists.

The final objective function is a combination of the cross-entropy loss function for the matching layer ( $\mathcal{L}_{match}$ ) and the duplicate-aware cross-entropy loss functions for each encoder and decoder layer:

$$\mathcal{L} = \mathcal{L}_{match} + \sum_k \mathcal{L}_{attn}^{enc_k} + \sum_k \mathcal{L}_{attn}^{dec_k}, \quad (13)$$

Approach	Online	AssA	FragA	DetA	HOTA	MOTA	mAP
CorrTrack [11]	✓	58.02	57.75	45.48	51.13	63.0	72.3
CorrTrack w. ReID [11]	✓	60.21	59.66	46.56	52.71	63.8	72.7
Tracktor++ [3] w. Poses [11]	✓	59.41	58.61	46.30	52.21	63.3	71.4
Tracktor++ [3] w. Correspondences [11]	✓	54.05	52.02	44.67	48.90	61.6	<b>73.6</b>
Ours	✓	<b>62.20</b>	<b>60.93</b>	<b>47.20</b>	<b>53.94</b>	<b>64.1</b>	<b>73.6</b>
CorrTrack [11]	✗	60.93	60.37	45.48	52.42	63.9	72.3

**Table 1.** Comparison to state-of-the-art methods on the PoseTrack21 dataset.

Method	AssA	DetA	LocA	HOTA	MOTA
TRMOT [52]	54.98	40.91	79.92	46.85	47.2
FairMOT [60]	61.45	47.43	83.16	53.53	56.3
Tracktor++ [3]	65.43	<b>52.71</b>	<b>83.09</b>	58.29	<b>59.5</b>
CorrTrack + ReID [11]	64.19	51.33	82.80	56.95	52.0
Ours	<b>66.89</b>	51.81	82.71	<b>58.42</b>	55.3

**Table 2.** Comparison to state-of-the-art methods on the PoseTrack21-MOT dataset.

where  $\mathcal{L}_{attn}^{enc_k}$  and  $\mathcal{L}_{attn}^{dec_k}$  represent the duplicate-aware cross-entropy loss functions for the  $k$ -th encoder and decoder layer, respectively.

## 4 Experiments

### 4.1 Datasets and Evaluation

We evaluate our work on the PoseTrack datasets [1, 11]. Both datasets are large-scale benchmarks for multi-person pose tracking and contain 593 videos for training and 170 for evaluation. The videos contain various activities and include highly diverse poses and severe occlusions as shown in Fig. 1. Since for PoseTrack 2018 the evaluation server is not anymore available, we only report results on the validation set. Compared to PoseTrack 2018, PoseTrack21 [11] provides more annotations and additional benchmarks for multi-object tracking (MOT) and person search. We thus primarily focus on PoseTrack21 [11] in our experiments. For evaluation, we use *keypoint HOTA* [11]. Keypoint HOTA consists of sub-metrics that measure the *detection accuracy* (*DetA*), the *association accuracy* (*AssA*) and the *fragmentation accuracy* (*FragA*). In addition, we report results for the *keypoint-based MOTA* metric [1]. Both metrics are evaluated on a keypoint level and then averaged. For completeness, we report the keypoint detection performances in terms of *mean average precision* (*mAP*).

We follow common practice [42, 54, 38, 55, 11, 49] and utilize a multi-frame pose estimation approach to compensate for missed detections due to motion blur and occlusions during inference. In particular, we utilize keypoint correspondences as in [38, 11]. In the following, we compare our approach to the state-of-the-art. Implementation details and detailed ablation studies are provided as **supplementary material**.

### 4.2 Comparison with State-of-the-Art

**PoseTrack21:** We first evaluate our model on the PoseTrack21 validation set and compare the performance to methods proposed in [11] using the keypoint

HOTA [11] and the MOTA metrics [1]. The results are shown in Table 1. Our proposed pose tracker consistently outperforms existing methods, achieving a HOTA score of 53.94 and a MOTA score of 64.1. Compared to CORRTRACK W. REID, our approach boosts the association accuracy (AssA) and fragmentation accuracy (FragA) by +1.99% and +1.27% to 62.20 and 60.93, respectively. Additionally, the detection accuracy (DetA) and the mAP increase to 47.20 and 73.6, respectively. While our approach performs online multi-person pose tracking, it also outperforms the offline approach CorrTrack.

We further evaluate our approach on the PoseTrack21-MOT benchmark and compare the performance to the methods in [11]. As we show in Table 2, our approach consistently outperforms existing methods in terms of AssA (66.89) and HOTA (58.42). Tracktor++ [3] achieves a slightly higher DetA and localization accuracy (LocA), which also results in higher MOTA. While Tracktor++ has been trained on the annotated bounding boxes for MOT, our approach has been trained for pose tracking and we simply generate the bounding boxes from the estimated poses. Consequently, MOT methods achieve a better MOTA score due to higher bounding box detection and localization accuracy. As discussed in [32], HOTA is a better metric than MOTA for MOT.

In the supplementary material, we provide detailed ablation studies on PoseTrack21, which include the impact of the loss terms, encoder, confidence-guided track updates, new track embedding head and the hyperparameters  $\alpha$ ,  $\tau_{dup}$  and  $\tau_{age}$ .

**PoseTrack 2018:** The comparison with related works on PoseTrack 2018 is difficult for two reasons: i) The PoseTrack 2018 dataset is not available anymore and it is no longer possible to submit results to the official test server; ii) the validation set was released in two different versions. The first version (v1) contains 74 whereas the second version (v2) contains 170 sequences, respectively. For a better comparability, we grouped related works by the version of the used validation set in Table 3. The results for CorrTrack [38] show that the version v2 is much more difficult. Compared to CorrTrack, our method improves the MOTA score by 0.9% to 64.5. The pose estimation performance increases from 75.9 to 76.4 in terms of mAP. Our works performs similar to [13] in terms of MOTA while achieving a higher mAP. CombDet [49] achieves a higher accuracy, but it uses a stronger multi-frame person detector and is an offline approach, whereas our approach is an online approach. LDGNN [55] also uses a better multi-frame pose estimator, but the code is not publicly available.

**Market1501:** For a comparison with related works on person re-identification, we train our proposed person re-identification model SPADPE (Section 3.2) on the Market1501 dataset [62]. Market1501 is a small dataset for person re-identification and contains 32,688 annotated bounding boxes with a total of 1501 identities. The training and testing sets consist of 751 and 750 identities, respectively. As this dataset does not provide annotated keypoints, we utilize our pose estimator trained on PoseTrack21 to estimate the human pose of all person crops of Market1501. For the evaluation of the person re-identification model, we follow [62] and report the mean average precision (mAP) and rank-1 metrics.

Approach	Online	Val. Set	Detector	MOTA	mAP
STAF [37]	✓	v1	-	60.9	70.4
T CPN++ [57]	✓	v1	Cascade R-CNN [4]	64.0	80.9
MIPAL [22]	✓	v1	-	65.7	74.6
KeyTrack [42]	✓	v1	HTC [7]	66.6	81.6
CorrTrack [38]	✓	v1	Cascade R-CNN [4]	68.8	79.2
TKMRNet [63]	✓	v1	Faster R-CNN FPN DCN [64]	68.9	76.7
CorrTrack [38]	✗	v1	Cascade R-CNN [4]	69.1	79.2
CorrTrack [38]	✓	v2	Cascade R-CNN [4]	63.6	75.9
LTIVA [13]	✓	v2	-	64.7	71.4
CombDet [49]	✗	v2	ResNet-101 SNIPER [41]	68.7	81.5
LDGNN [55]	✓	v2	Faster R-CNN FPN DCN [64]	69.2	77.9
Ours	✓	v2	Cascade R-CNN [4]	64.5	76.4

**Table 3.** Comparison to the state-of-the-art on PoseTrack 2018 [1]. Two versions of the validation set have been released containing 74 (v1) and 170 (v2) sequences, respectively.

Metric	PSE [40]	GLAD [53]	PGFA [34]	PCB [45]	OAMN [8]	HOReID [48]	FED [51]	BPBreID <sub>RN</sub> [43]	PAT [28]
r = 1	87.7	89.9	91.2	92.3	92.3	94.2	95.0	95.1	95.4
mAP	69.0	73.9	76.8	77.4	79.8	84.9	86.3	87.0	88.0
	NGFR [58]	TransReID [18]	RFCNet [21]	PFD [50]	FPC [56]	DIP [25]	BoT [33]	DC-Former [27]	Ours
r = 1	95.5	95.0	95.2	95.5	95.1	95.6	95.4	<b>96.0</b>	<u>95.8</u>
mAP	88.1	88.2	89.2	89.7	91.4	90.3	<b>94.2</b>	90.4	<u>92.8</u>

**Table 4.** Comparison of SPADPE (ours) to state-of-the-art methods on Market1501 [62]. The best results are **bold** and the second best results are underlined.

Since Market1501 contains pedestrians with very limited pose variations, it is not expected that our approach achieves state-of-the-art results on Market1501. Nevertheless, the results are on par with the state-of-the-art as shown in Table 4. We evaluate SPADPE on PoseTrack21 in the supplementary material.

## 5 Conclusion

We presented a novel approach for multi-person pose tracking that can be combined with any off-the-shelf multi-person human pose estimator. Our method employs a duplicate-aware association and dynamically weights the impact of temporal pose similarities and appearance-based similarities based on the attention probabilities of each similarity measure. We evaluated our approach on the challenging PoseTrack21 dataset where our approach outperforms previous works for multi-person pose tracking. On PoseTrack 2018, the approach is only outperformed by methods that use a more expensive human pose estimator. We also evaluated the proposed Spatially Adaptive Pose DEnormalization (SPAPDE) for the task of person re-identification on PoseTrack21 and the less challenging Market1501 dataset where our approach performs on par with the state-of-the-art.

## Appendix

### A Implementation Details

*Track Embedding and Edge Embedding Heads:* Fig. 4 visualizes the structure of the proposed track embedding head (Fig. 4a) and the edge embedding head (Fig. 4b). The new track embedding head has the same structure as the track embedding head.

*Re-Identification Model:* We train our re-identification model for 244 epochs on the PoseTrack21 person search dataset with a batch size of 256 and a learning rate of 0.00035 that we decay to 0.000035 after 75 epochs. During the first 10 epochs, we apply a linear learning rate warm-up. Additionally, we apply data augmentation such as random scaling, random rotation and horizontal flipping.

*Dual-Source Attention Transformer:* Our proposed dual-source transformer employs two encoder and two decoder stages. On the PoseTrack21 dataset, we train our transformer for 14 epochs with a learning rate of 0.0001, which is decayed by a factor of 10 after 13 epochs. We further incorporate a linear learning rate warm-up over the course of 16k iterations and optimize the network with the AdamW [31] optimizer. Each training sequence is split into sub-sequences of length three with an overlap of one frame. We follow the same settings on the PoseTrack 2018 dataset and train the dual-source transformer for 11 epochs.

*Person Detector:* For a fair comparison to related works, we utilize the same person detector and pose estimation model for all our experiments. In particular, we use the person detector from [11], which consists of a FasterRCNN [39] with a ResNet50-FPN [29] backbone. The detector was first pre-trained on MSCOCO [30] and further fine-tuned on PoseTrack21 for 30 more epochs. As pose estimator, we employ the released model [11], that was originally proposed in [38]. The pose estimation model was trained on MSCOCO and PoseTrack21 for 215 and 16 epochs, respectively. On PoseTrack 2018, we use Cascade R-CNN [4] as object detector and the pose estimator from CorrTrack [38].

### B Ablation Studies

We perform ablation experiments to examine the influence of each building block of our proposed method. All experiments are conducted on the PoseTrack21 dataset.

#### B.1 Evaluation of the Network Architecture

*Loss terms, Encoder and Confidence-Guided Track Update:* We first evaluate the impact of each component in our tracking model on the keypoint HOTA

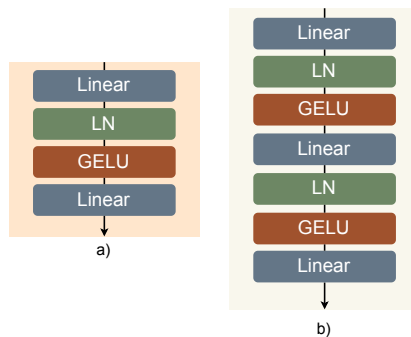


Fig. 4. Illustration of the a) track embedding head and b) edge embedding head.

$\mathcal{L}_{attn}^{dec}$	Encoder	$\mathcal{L}_{attn}^{enc}$	CG-Update	HOTA
				53.04
✓				53.40
✓	✓			53.56
✓	✓	✓		53.61
✓	✓	✓	✓	53.94

Table 5. Impact of several components in our pose tracking network on the tracking performance. CG-Update denotes the Confidence-Guided Track Update as discussed in Section 3.1.

score [11] in Table 5. As our base model, we start with the dual-source decoder with matching layer that we trained with the matching loss  $\mathcal{L}_{match}$ , *i.e.* (11). Subsequently, we incrementally activate several components and evaluate their impact on the overall performance. Direct supervision on the dual-source attention layers using  $\mathcal{L}_{attn}^{dec}$  ((12)) increases the overall performance from 53.04 to 53.40 in terms of HOTA. Using additional transformer encoder layers (Fig. 2a) boosts the performance to 53.56. Using the loss  $\mathcal{L}_{attn}^{enc}$  (12) also for the encoder increases HOTA to 53.61. The impact of the Confidence-Guided Track Update (Section 3.1) is shown in the last row. It further increases the tracking performance by 0.33 to a HOTA score of 53.94.

*Re-Identification Model and Edge Features:* To evaluate the impact of the re-identification network, we trained our tracking model with two different re-identification networks. We used the proposed SPAPDE network (Section 3.2) and the re-identification network [33], which we term RESNET50 & BOT. The first and last row in Table 6 show that adding Spatially Adaptive Pose Denormalization layers (SPAPDE) to the network increases HOTA from 53.47 to 53.94. Furthermore, Table 6 shows the impact of different embedded pose similarities. IoU only provides coarse information and does not allow to distinguish between spatially closely located person instances. Even though a temporal similarity based on IoU achieves a HOTA score of 53.59 and outperforms all related

Re-ID Backbone	SPAPDE	Temporal Person Similarity	HOTA
ResNet50 & BoT		IoU + OKS	53.47
ResNet50 & BoT	✓	IoU	53.59
ResNet50 & BoT	✓	OKS	53.81
ResNet50 & BoT	✓	IoU + OKS	53.94

**Table 6.** We evaluate the impact of different re-identification backbones and different temporal person similarities used for the calculation of edge embeddings.

Track Embedding Initialization	AssA	FragA	DetA	HOTA
New Track Embedding Head	62.20	60.93	47.20	53.94
Detection Embedding	61.87	60.73	47.15	53.76

**Table 7.** Impact of the New Track Embedding Head on the overall tracking performance on PoseTrack21.

works (Table 1), OKS-based temporal similarity performs better and the combination performs best.

*New Track Embedding Head:* Given detections in frame  $t$  that can not be matched to any existing track, we use the New Track Embedding Head (Figure 2d) to generate new track embeddings from the unmatched detection embeddings. In Table 7, we evaluate the impact of the *New Track Embedding Head* compared to initializing new tracks directly from the detection embeddings. The *New Track Embedding Head* provides a better initialization of the track embeddings.

*Edge Embedding Update:* To update the edge embeddings, we utilize an  $\alpha$ -Gate to weight the contributions of the appearance-based and edge-based attention logits (eq. (5)). While we evaluate the impact of  $\alpha$  in Figure 5, Table 8 shows that learning  $\alpha$  does not improve the results. We further evaluate the tracking performance when the fusion is not done at the logits, *i.e.*, before the softmax, but after the softmax as in (2), *i.e.*,

$$\widehat{E}_{T \rightarrow D}^t = FFN_E(A_{:, :-1}), \quad (14)$$

where  $A_{:, :-1}$  denotes the attention weights without the last column (Section 3.1). The last row in Table 8 shows that the performance largely decreases from a HOTA score of 53.94 to 50.53 in this case.

## B.2 Hyperparameter Evaluation on PoseTrack21

*Impact of  $\alpha$ :* We evaluate the impact of  $\alpha$  in the  $\alpha$ -Gate ((2) and (5)) in Fig. 5a.  $\alpha$  weights the contribution of the appearance-based attention weights and the pose-based attention weights, where  $\alpha = 1.0$  only considers appearance-based

Edge Embedding Update	Learnable $\alpha$	AssA	FragA	DetA	HOTA
$\alpha$ -gated attention logits	✓	62.20	60.93	47.20	53.94
$\alpha$ -gated attention logits		61.80	60.59	47.15	53.74
$\alpha$ -gated attention weights		54.74	50.77	47.14	50.53

**Table 8.** Impact of updating edge embeddings based on  $\alpha$ -gated attentions weights or attention logits on the overall tracking performance on PoseTrack21.

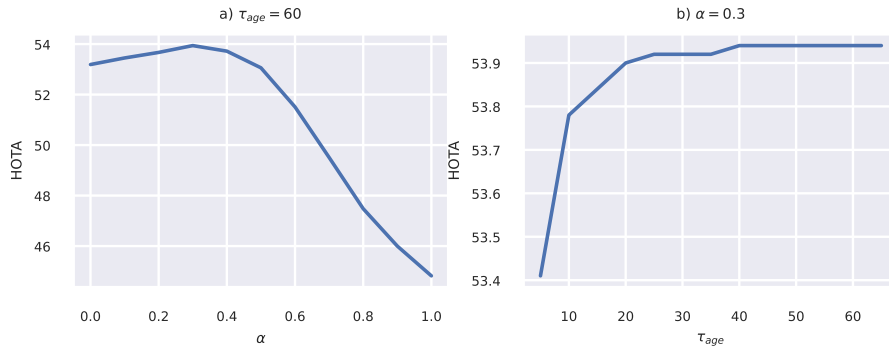


**Fig. 5.** Impact of the parameters  $\alpha$  and maximum track ages  $\tau_{age}$  on the tracking performance. a) visualizes the impact of  $\alpha$  with  $\tau_{age} = 60$  and  $\tau_{dup} = 0.4$ . b) shows the performance evaluation with respect to the maximum track age  $\tau_{age}$  with  $\alpha = 0.3$  and  $\tau_{dup} = 0.4$ .

attention weights and, vice versa,  $\alpha = 0.0$  only considers edge-based attention weights. As we can observe in Fig. 5a, the tracking performance drastically decreases for  $\alpha > 0.4$ . Appearance-based person features are very sensitive to persons with similar appearance as it is common in sports videos, resulting in false associations and a high degree of identity switches. For  $0 \leq \alpha \leq 0.3$ , we can observe a linear increase in the overall performance, peaking at  $\alpha = 0.3$ , which we used in all other experiments. This shows that pose-based and appearance-based similarities complement each other. Pose similarities provide strong guidance between consecutive frames, while appearance-based features allow to recover inactive tracks, *e.g.*, due to occlusion.

*Impact of  $\tau_{age}$ :* We close tracks that have not been tracked for more than  $\tau_{age}$  frames and do not include them for the detection-to-track matching anymore. Fig. 5b shows that the accuracy saturates at  $\tau_{age} = 40$ . We used  $\tau_{age} = 60$  in all other experiments.

*Impact of  $\tau_{dup}$ :* During tracking, we remove unmatched detections if they have a matching confidence  $m_{ij} > \tau_{dup}$  with an already matched track (Section 3.1).



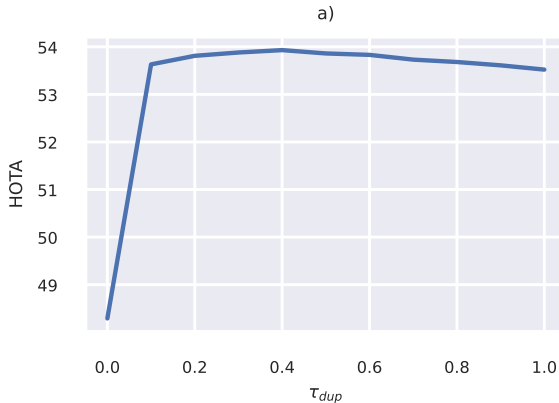


**Fig. 6.** Evaluation of the duplicate confidence threshold  $\tau_{dup}$  with  $\alpha = 0.3$  and  $\tau_{age} = 60$ .

Fig. 6 shows that the accuracy drops without such a threshold since duplicates generate new tracks in this case. We use  $\tau_{dup} = 0.4$ .

## C Person Re-Identification

We finally evaluate the person re-identification model on PoseTrack21 and measure the performance in terms of mean average precision (mAP), *i.e.*, we calculate the area under the Precision-Recall curve for each query and average over all queries. As we show in Table 9, training a ResNet50 [17] with proper data sampling results in a significant performance gain and results in a mAP score of 68.65. In more detail, we sample  $K = 6$  different instances of the same person identity for every batch. Surprisingly, training the ResNet50 from scratch results in a better mAP performance (68.65) compared to training a ResNet50 pre-trained on ImageNet [9] (68.31). As discussed in Section 3.3, we follow [33], which further increases the performance to 73.78. To incorporate pose information, we replace each batch normalization layer by SPAPDE layers (eq. (9)), which incorporates pose information by the keypoint heatmaps. The best performance is achieved by using keypoint heatmaps with a kernel size of 10. Specifically, we denote the kernel size as the standard deviation of a Gaussian distribution. For each keypoint we calculate a Gaussian distribution with the mean set to the respective keypoint location and a standard deviation of 10. Further following [33], we achieve a total performance of 78.0 and 74.42 with ground truth and estimated poses, respectively. By adding SPAPDE, mAP thus increases from 73.78 to 74.42.

Model	GT Poses	Kernel Width	Sampling	pre-trained	mAP	loss
ResNet50				✓	64.24	triplet
ResNet50			✓	✓	68.31	triplet
ResNet50			✓		68.65	triplet
ResNet50 & back-of-tricks [33]			✓		73.38	triplet + ce + center
SPAPDE ResNet50	✓	2	✓		66.77	triplet
SPAPDE ResNet50	✓	5	✓		70.39	triplet
SPAPDE ResNet50	✓	10	✓		71.17	triplet
SPAPDE ResNet50	✓	15	✓		69.62	triplet
SPAPDE ResNet50 & bag-of-tricks [33]	✓	10	✓		<b>78.00</b>	triplet + ce + center
SPAPDE ResNet50 & bag-of-tricks [33]		10	✓		<b>74.42</b>	triplet + ce + center

**Table 9.** We evaluate the person re-identification performance (mAP) on the PoseTrack21 dataset for various model settings.

## References

1. Andriluka, M., Iqbal, U., Milan, A., Insafutdinov, E., Pishchulin, L., Gall, J., Schiele, B.: PoseTrack: A Benchmark for Human Pose Estimation and Tracking. In: CVPR (2018)
2. Ba, J.L., Kiros, J.R., Hinton, G.E.: Layer Normalization (2016)
3. Bergmann, P., Meinhardt, T., Leal-Taixé, L.: Tracking without bells and whistles. In: ICCV (2019)
4. Cai, Z., Vasconcelos, N.: Cascade R-CNN: High Quality Object Detection and Instance Segmentation. arXiv preprint arXiv:1906.09756 (2019)
5. Chen, D., Li, H., Xiao, T., Yi, S., Wang, X.: Video person re-identification with competitive snippet-similarity aggregation and co-attentive snippet embedding. CVPR (2018)
6. Chen, D., Doering, A., Zhang, S., Yang, J., Gall, J., Schiele, B.: Keypoint message passing for video-based person re-identification. In: AAAI (2021)
7. Chen, K., Pang, J., Wang, J., Xiong, Y., Li, X., Sun, S., Feng, W., Liu, Z., Shi, J., Ouyang, W., Loy, C.C., Lin, D.: Hybrid Task Cascade for Instance Segmentation. CVPR (2019)
8. Chen, P., Liu, W., Dai, P., Liu, J., Ye, Q., Xu, M., Chen, Q., Ji, R.: Occlude them all: Occlusion-aware attention network for occluded person re-id. In: ICCV (2021)
9. Deng, J., Dong, W., Socher, R., Li, L.J., Li, K., Fei-Fei, L.: Imagenet: A large-scale hierarchical image database. In: CVPR (2009)
10. Dijkstra, E.W.: A note on two problems in connexion with graphs. *Numerische Mathematik* (1959)
11. Doering, A., Chen, D., Zhang, S., Schiele, B., Gall, J.: PoseTrack21: A Dataset for Person Search, Multi-Object Tracking and Multi-Person Pose Tracking. In: CVPR (2022)
12. Doering, A., Iqbal, U., Gall, J.: Joint Flow: Temporal Flow Fields for Multi Person Tracking. CVPR (2018)
13. Fu, Y., Liu, S., Iqbal, U., Mello, S.D., Shi, H., Kautz, J.: Learning to Track Instances without Video Annotations. CVPR (2021)
14. Gao, S., Wang, J., Lu, H., Liu, Z.: Pose-guided Visible Part Matching for Occluded Person ReID. In: CVPR (2020)
15. Girdhar, R., Gkioxari, G., Torresani, L., Paluri, M., Tran, D.: Detect-and-Track: Efficient Pose Estimation in Videos. In: CVPR (2018)

16. Gong, L., Cheng, Q.: Exploiting Edge Features for Graph Neural Networks. In: CVPR (2019)
17. He, K., Zhang, X., Ren, S., Sun, J.: Deep Residual Learning for Image Recognition. In: CVPR (2016)
18. He, S., Luo, H., Wang, P., Wang, F., Li, H., Jiang, W.: Transreid: Transformer-based object re-identification. In: CVPR (2021)
19. Hendrycks, D., Gimpel, K.: Gaussian Error Linear Units (GELUs). arXiv-Preprint (2016)
20. Hermans, A., Beyer, L., Leibe, B.: In Defense of the Triplet Loss for Person Re-Identification. arXiv-Preprint (2017)
21. Hou, R., Ma, B., Chang, H., Gu, X., Shan, S., Chen, X.: Feature Completion for Occluded Person Re-Identification. TPAMI (2020)
22. Hwang, J., Lee, J., Park, S., Kwak, N.: Pose estimator and tracker using temporal flow maps for limbs. In: IJCNN (2019)
23. Ioffe, S., Szegedy, C.: Batch Normalization: Accelerating Deep Network Training by Reducing Internal Covariate Shift. In: ICML (2015)
24. Jin, S., Liu, W., Ouyang, W., Qian, C.: Multi-person Articulated Tracking with Spatial and Temporal Embeddings. CVPR (2019)
25. Li, D., Chen, S., Zhong, Y., Liang, F., Ma, L.: DiP: Learning Discriminative Implicit Parts for Person Re-Identification. In: arXiv-Preprint (2022)
26. Li, J., Zhang, S., Huang, T.: Multi-Scale 3D Convolution Network for Video Based Person Re-Identification. In: AAAI (2019)
27. Li, W., Zou, C., Wang, M., Xu, F., Zhao, J., Zheng, R., Cheng, Y., Chu, W.: DCFormer: Diverse and Compact Transformer for Person Re-Identification. AAAI (2023)
28. Li, Y., He, J., Zhang, T., Liu, X., Zhang, Y., Wu, F.: Diverse part discovery: Occluded person re-identification with part-aware transformer. In: CVPR (2021)
29. Lin, T.Y., Dollár, P., Girshick, R.B., He, K., Hariharan, B., Belongie, S.J.: Feature Pyramid Networks for Object Detection. In: CVPR (2017)
30. Lin, T.Y., Maire, M., Belongie, S., Hays, J., Perona, P., Ramanan, D., Dollár, P., Zitnick, C.L.: Microsoft COCO: Common Objects in Context. In: ECCV (2014)
31. Loshchilov, I., Hutter, F.: Decoupled Weight Decay Regularization. In: ICCV (2019)
32. Luiten, J., Osep, A., Dendorfer, P., Torr, P., Geiger, A., Leal-Taixé, L., Leibe, B.: HOTA: A Higher Order Metric for Evaluating Multi-Object Tracking. IJCV (2020)
33. Luo, H., Gu, Y., Liao, X., Lai, S., Jiang, W.: Bag of Tricks and a Strong Baseline for Deep Person Re-Identification. In: CVPRW (2019)
34. Miao, J., Wu, Y., Liu, P., Ding, Y., Yang, Y.: Pose-guided feature alignment for occluded person re-identification. In: ICCV (2019)
35. Park, T., Liu, M., Wang, T., Zhu, J.: Semantic Image Synthesis With Spatially-Adaptive Normalization. In: CVPR (2019)
36. Qi, L., Huo, J., Wang, L., Shi, Y., Gao, Y.: MaskReID: A Mask Based Deep Ranking Neural Network for Person Re-identification. ICME (2018)
37. Raaj, Y., Idrees, H., Hidalgo, G., Sheikh, Y.: Efficient Online Multi-Person 2D Pose Tracking with Recurrent Spatio-Temporal Affinity Fields. CVPR (2019)
38. Rafi, U., Doering, A., Leibe, B., Gall, J.: Self-supervised Keypoint Correspondences for Multi-Person Pose Estimation and Tracking in Videos. In: ECCV (2020)
39. Ren, S., He, K., Girshick, R.B., Sun, J.: Faster R-CNN: Towards Real-Time Object Detection with Region Proposal Networks. In: NeurIPS (2015)

40. Sarfraz, M.S., Schumann, A., Eberle, A., Stiefelhagen, R.: A Pose-Sensitive Embedding for Person Re-Identification with Expanded Cross Neighborhood Re-Ranking. CVPR (2018)
41. Singh, B., Najibi, M., Davis, L.S.: SNIPER: Efficient Multi-Scale Training. NeurIPS (2018)
42. Snower, M., Kadav, A., Lai, F., Graf, H.P.: 15 Keypoints Is All You Need. CVPR (2020)
43. Somers, V., De Vleeschouwer, C., Alahi, A.: Body Part-Based Representation Learning for Occluded Person Re-Identification. WACV (2023)
44. Sun, Y., Xu, Q., Li, Y., Zhang, C., Li, Y., Wang, S., Sun, J.: Perceive Where to Focus: Learning Visibility-aware Part-level Features for Partial Person Re-identification. CVPR (2019)
45. Sun, Y., Zheng, L., Yang, Y., Tian, Q., Wang, S.: Beyond Part Models: Person Retrieval with Refined Part Pooling (and A Strong Convolutional Baseline). In: ECCV (2018)
46. Szegedy, C., Vanhoucke, V., Ioffe, S., Shlens, J., Wojna, Z.: Rethinking the Inception Architecture for Computer Vision. In: CVPR (2016)
47. Vaswani, A., Shazeer, N., Parmar, N., Uszkoreit, J., Jones, L., Gomez, A.N., Kaiser, L.u., Polosukhin, I.: Attention is All you Need. In: NeurIPS (2017)
48. Wang, G., Yang, S., Liu, H., Wang, Z., Yang, Y., Wang, S., Yu, G., Zhou, E., Sun, J.: High-order information matters: Learning relation and topology for occluded person re-identification. In: CVPR (2020)
49. Wang, M., Tighe, J., Modolo, D.: Combining detection and tracking for human pose estimation in videos. CVPR (2020)
50. Wang, T., Liu, H., Song, P., Guo, T., Shi, W.: Pose-guided feature disentangling for occluded person re-identification based on transformer. In: AAAI (2022)
51. Wang, Z., Zhu, F., Tang, S., Zhao, R., He, L., Song, J.: Feature Erasing and Diffusion Network for Occluded Person Re-Identification. In: CVPR (2022)
52. Wang, Z., Zheng, L., Liu, Y., Wang, S.: Towards Real-Time Multi-Object Tracking. ECCV (2020)
53. Wei, L., Zhang, S., Yao, H., Gao, W., Tian, Q.: GLAD: Global-Local-Alignment Descriptor for Pedestrian Retrieval. ICM (2017)
54. Xiao, B., Wu, H., Wei, Y.: Simple Baselines for Human Pose Estimation and Tracking. ECCV (2018)
55. Yang, Y., Ren, Z., Li, H., Zhou, C., Wang, X., Hua, G.: Learning Dynamics via Graph Neural Networks for Human Pose Estimation and Tracking. CVPR (2021)
56. Ye, Y., Zhou, H., Yu, J., Hu, Q., Yang, W.: Dynamic Feature Pruning and Consolidation for Occluded Person Re-Identification. ArXiv-Preprint (2022)
57. Yu, D., Su, K., Sun, J., Wang, C.: Multi-person Pose Estimation for Pose Tracking with Enhanced Cascaded Pyramid Network. In: ECCVW (2018)
58. Yu, S., Chen, D., Zhao, R., Chen, H., Qiao, Y.: Neighbourhood-guided Feature Reconstruction for Occluded Person Re-Identification. ArXiv-Preprint (2021)
59. Zhang, R., Zhu, Z., Li, P., Wu, R., Guo, C., Huang, G., Xia, H.: Exploiting Offset-guided Network for Pose Estimation and Tracking. In: CVPRW (2019)
60. Zhang, Y., Wang, C., Wang, X., Zeng, W., Liu, W.: FairMOT: On the Fairness of Detection and Re-Identification in Multiple Object Tracking. ICCV (2021)
61. Zheng, L., Huang, Y., Lu, H., Yang, Y.: Pose-Invariant Embedding for Deep Person Re-Identification. IEEE Transactions on Image Processing (2019)
62. Zheng, L., Shen, L., Tian, L., Wang, S., Wang, J., Tian, Q.: Scalable Person Re-identification: A Benchmark. In: ICCV (2015)

63. Zhou, C., Ren, Z., Hua, G.: Temporal keypoint matching and refinement network for pose estimation and tracking. In: *ECCV* (2020)
64. Zhu, X., Hu, H., Lin, S., Dai, J.: Deformable ConvNets v2: More Deformable, Better Results. *arXiv preprint arXiv:1811.11168* (2018)